

Leveraging ASIC AI Chips for Homomorphic Encryption

Jianming Tong
jianming.tong@gatech.edu
Georgia Institute of Technology
Atlanta, Georgia, USA

Tianhao Huang
tianhaoh@mit.edu
Massachusetts Institute of Technology
Cambridge, Massachusetts, USA

Leo de Castro
ldec@mit.edu
Massachusetts Institute of Technology
Cambridge, Massachusetts, USA

Anirudh Itagi
aitagi7@gatech.edu
Georgia Institute of Technology
Atlanta, Georgia, USA

Jingtian Dang
dangjingtian@gatech.edu
Georgia Institute of Technology
Atlanta, Georgia, USA

Anupam Golder
anupamgolder@gatech.edu
Georgia Institute of Technology
Atlanta, Georgia, USA

Asra Ali
asraa@google.com
Google
Austin, Texas, USA

Jevin Jiang
jevinjiang@google.com
Google
Sunnyvale, California, USA

Arvind
arvind@mit.edu
Massachusetts Institute of Technology
Cambridge, Massachusetts, USA

G. Edward Suh*
suh@ece.cornell.com
Cornell University/NVIDIA
Ithaca, New York, USA

Tushar Krishna
tushar@ece.gatech.edu
Georgia Institute of Technology
Atlanta, Georgia, USA

Abstract

Cloud-based services are making the outsourcing of sensitive client data increasingly common. Although homomorphic encryption (HE) offers strong privacy guarantee, it requires substantially more resources than computing on plaintext, often leading to unacceptably large latencies in getting the results. HE accelerators have emerged to mitigate this latency issue, but with the high cost of ASICs. In this paper we show that HE primitives can be converted to AI operators and accelerated on existing ASIC AI accelerators, like TPUs, which are already widely deployed in the cloud. Adapting such accelerators for HE requires (1) supporting modular multiplication, (2) high-precision arithmetic in software, and (3) efficient mapping on matrix engines. We introduce the CROSS compiler (1) to adopt Barrett reduction to provide modular reduction support using multiplier and adder, (2) Basis Aligned Transformation (BAT) to convert high-precision multiplication as low-precision matrix-vector multiplication, (3) Matrix Aligned Transformation (MAT) to convert Number Theoretic Transformation into layout-invariant matrix multiplication that can be efficiently processed on 2D spatial matrix engine. Our evaluation of CROSS on a Google TPUv4 demonstrates significant performance improvements, with up to 161× and 5× speedup compared to the previous work on many-core CPUs and V100. The kernel-level codes are open-sourced at https://github.com/google/jaxite/tree/main/jaxite_word.

1 Introduction

Artificial intelligence (AI) is rapidly evolving and often exceeds human capabilities in diverse applications. Examples

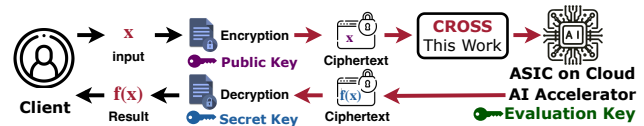


Figure 1. HE enables direct computation on encrypted data to enable privacy-preserving model serving.

include large language models that excel in complex reasoning and diffusion models that generate creative contents [8, 43, 46, 63]. In order to utilize sensitive or private data for AI, we need strong confidentiality protection for the AI serving life-cycle even in untrusted environments. Homomorphic Encryption (HE) promises strong end-to-end confidentiality by enabling data processing in an encrypted form, as shown in Fig. 1. However, HE inflates data sizes by 200× and computation by 10,000×, resulting in a 1000× slowdown on a multi-core CPU [11, 47, 53, 54].

While HE’s inherent parallelism seems tailor-made for dedicated ASICs [2, 38, 39, 41, 49, 54, 55, 57, 61, 62], the cost of designing, verifying, and maintaining such an ASIC is daunting, often requiring years and millions of dollars. HE implementations on CPUs, GPUs, and FPGAs have made significant strides recently but still fall short of ASICs’ performance by at least 20× [3, 4, 11, 13, 20, 23, 36, 50–52, 56, 59, 66].

To reduce this performance gap without fabricating a custom ASIC only for HE, this paper studies opportunities and challenges in accelerating HE using existing ASICs for Artificial Intelligence (AI), which are already pervasive in the cloud [24, 25, 31]. We propose a compilation framework, **CROSS**¹, to enable HE deployment on AI accelerators.

*This work was done before the author joined NVIDIA.

¹Compiling Real-time Online Secure Service on ASIC AI Accelerators

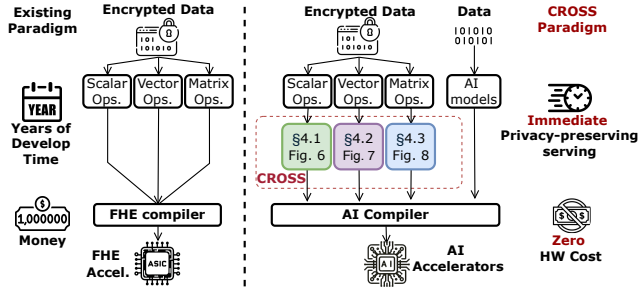


Figure 2. CROSS enables real-time HE serving on existing AI accelerators without hardware modifications.

The following characteristics of AI accelerators make accelerating HE feasible: (1) mix of vector processing unit and matrix multiplication unit that combine to provide a high throughput via a massive number of arithmetic units ($\geq 10^5$ MACs), (2) large amounts of programmable on-chip memory (≥ 100 MB), and (3) on-chip transpose/shuffling unit to enable parallel irregular memory access.

However, *functionally*, an AI accelerator lacks two features that enable ASIC HE accelerators use to run HE workloads: (1) support for modular arithmetic and (2) high-precision arithmetic (most AI inference accelerators only support 8-bit integer operations). To bridge these gaps, we implement Barrett reduction [12] to facilitate modular operations using existing multiplication, addition, and shift capabilities of AI accelerators. To further enable high precision, we propose chunk decomposition to decompose high-precision data into many low-precision chunks and convert the original high-precision operation into low-precision chunkwise multiplication and reduction.

Despite enabling functional correctness of HE processing in AI accelerators, several challenges hinder *optimal performance*: (1) decomposing a high-precision modular operation into many low-precision chunkwise operations introduces extra on-chip data movement, reducing performance for memory-bounded HE operations, (2) the rigid-shape 2D systolic array in AI accelerators only favors large-scale matrix multiplications, resulting in low computation resource utilization when processing vectorized HE operations including Number Theoretic Transform (NTT) and BasisChange.

To further gain performance, we propose two mapping optimizations in our compiler, CROSS. (1) *Basis Aligned Transformation (BAT)* schedules chunkwise multiplications as dense matrix multiplications. By aligning the additional on-chip data movements with the native datapath of AI accelerators, BAT maximizes data reuse and computational efficiency. (2) *Matrix Aligned Transformation (MAT)* reformats both the computation and data layouts of vectorized operations from NTT/INTT into layout-invariant matrix forms. These matrix representations are then transformed into larger low-precision matrix multiplications through BAT. Leveraging the synergy between BAT and MAT, CROSS enhances overall compute utilization of both vector processing units and

matrix multiplication units in AI accelerators while reducing memory accesses and on-chip memory storage requirements.

To the best of our knowledge, CROSS represents the first work to investigate deployment of HE workloads on AI accelerators, introducing a new paradigm of AI/HE co-acceleration on the same hardware substrate (see Fig. 2).

CROSS shows that AI accelerators without any additional hardware support can indeed be used to accelerate HE workloads that require no bootstrapping.

Our evaluation of HE implementation on Google TPUv4 shows that we can achieve as much as a 12 \times speedup over Lattigo [47] on a CPU, 5 \times speedup over a previous GPU implementation (100 \times [34]) on an NVIDIA V100, and 1.05 \times speedup over an FPGA implementation (Xilinx U280 [3]). While still approximately 50 \times slower than a well-designed HE ASIC, the lack of commercial HE chips and the widespread availability of TPU-like AI accelerators make our approach highly compelling. The primary performance gap with HE ASICs stems from (1) the absence of low-cost data shuffling engine, (2) the support of general moduli choice, and (3) less overall memory/compute, as discussed in §6.4.

This result suggests that HE acceleration on ASIC AI accelerators is a promising direction to investigate. ASIC AI accelerators can provide significantly higher HE performance compared to CPUs and be competitive to other programmable accelerators such as GPUs and FPGAs. We note that the current experimental results do not include bootstrapping, which may be required for large applications, and the HE performance on GPUs and FPGAs can also be improved with optimizations. For example, a more recent study (Cheddar [37]) on GPU-based HE acceleration reports higher HE performance on an NVIDIA A100. In that sense, fully understanding the potential of AI accelerators for complex HE applications with bootstrapping and the detailed comparisons across different programmable accelerators will need further studies.

We make the following contributions in this paper:

- A systematic characterization of HE operators consisting of (1) computation analysis and latency profiling of various HE operators, identifying NTT/INTT, Basis Change, and element-wise multiplication as the key performance bottlenecks. These operators account for 74.5% ~ 92.3% of the overall latency under Brakerski/Fan-Vercauteren (BFV) and Cheon, Kim, Kim and Song (CKKS); (2) a programmer’s view of available functionalities inside ASIC AI accelerators. (3) the gap between workloads and hardware.

- A novel compilation framework, CROSS, to systematically lower HE kernels into hardware primitives on off-the-shelf AI accelerators without any hardware modifications. At its core, CROSS introduces *BAT*, a foundational set of arithmetic transformations that map high-precision scalar modular operations to low-precision hardware. Using BAT, CROSS achieves highly efficient vectorized modular operations (VecModOp) and modular matrix multiplication (ModMatMul),

which are critical for most HE kernels. For complex HE kernels like NTT, CROSS further proposes **MAT** to reformulate interleaved VecModOps with cross-coefficient reduction as ModMatMul, ensuring efficient execution.

- We conducted a comprehensive evaluation of the HE operators on TPUv4 across various practical security parameters. Our TPUv4 implementation achieved up to a $12\times$ speedup over a SotA CPU implementation (Lattigo [47]) on an Intel i5-6600k, a $5\times$ speedup over a GPU implementation on an NVIDIA V100 (100x [34]), a $1.5\times$ speedup over a GPU implementation on a NVIDIA A100 (TensorFHE [23]), a 50% slowdown over a GPU implementation on an NVIDIA A100 (Cheddar [37]), and a $1.05\times$ speedup over a SotA FPGA implementation (FAB [3]) on Xilinx Alevo U280. We note that A100s use a new technology node and have higher power consumption compared to TPUv4. These results demonstrate that AI accelerators like TPUv4 can perform HE operations competitively with SotA GPU and FPGA implementations, indicating a promising direction for further exploration, including computationally intensive tasks like bootstrapping.

2 Background and Motivation

In this section, we introduce the background for Homomorphic Encryption (HE) and discuss key potential of AI accelerators for HE acceleration.

2.1 Homomorphic Encryption Background

HE is a specialized form of public-key encryption that enables computations to be performed directly on encrypted data without revealing the underlying plaintext. In an HE system, the client exclusively holds a private decryption key, while a public encryption key is made available for data encryption. Additionally, an evaluation key is provided to the cloud or computing service to facilitate computations on the encrypted data. In HE, direct computation on the encrypted data will apply computation on the underlying messages, such that the entire computation is secured in the privacy-preserving manner as shown in Fig. 1.

2.1.1 Terminology and Data Representation. The security of HE schemes is based on the hardness of Ring Learning With Errors (RLWE) problem [45]. This is a problem over a polynomial ring $R_Q := \mathbb{Z}_Q[x]/(x^N+1)$, where N is a power of two. An element in R_Q is a polynomial of the form $a(x) = \sum_{j=0}^{N-1} a_j \cdot x^j$, where each coefficient a_j is an integer in $[0, Q-1]$ and the polynomial is reduced by x^N+1 .

2.1.2 Residue Number System (RNS). To achieve 128-bit security level, ciphertexts coefficients need high-precision, i.e. up to thousands of bits [5, 57], which are not natively supported by the 32-bit computational architectures in CPUs or GPUs. Naively, mapping high-precision data to low-precision computation unit requires two steps: (1) breaking high-precision

coefficients into low-precision chunks supported by computation units and (2) executing multiplicative operations across all pairs of chunks from two coefficients. This segmentation and *chunkwise multiplication* incur *quadratic* computational overheads.

To reduce such quadratic pair-wise computation costs, the Chinese Remainder Theorem (CRT) allows us to construct a set of coprime RNS basis $\{q_0, \dots, q_{L-1}\}$, where $Q = \prod_{i=0}^{L-1} q_i$. Under CRT, each high-precision coefficient $a_j, j \in [0, N-1]$ of a polynomial in R_Q is represented as residues of a sequence of L smaller moduli $\{a_j \bmod q_i\}$ for $i \in [0, L-1]$. These L obtained polynomials with low-precision coefficients are referred to as limbs, noted as $(\text{limb}_i), i \in [0, L-1]$. The isomorphism $R_Q \cong R_{q_0} \otimes \dots \otimes R_{q_{L-1}}$ allows addition and multiplication to be performed "limb-wise" over elements of R_Q . Thus, a limb of one polynomial multiplies only with its counterpart limb of another polynomial, reducing quadratic computational overhead down to linear. In the post-CRT ciphertext, different limbs get processed independently, facilitating limb-level parallelism. A summary of the notations is listed in Tab. 1.

However, RNS cannot directly reduce high-precision data to an arbitrary low precision due to inherent constraints. Specifically, RNS requires a set of moduli that (1) multiply to the original modulus Q , and (2) are pairwise co-prime. On typical AI accelerators [31, 33], the lowest supported precision is 8-bit integer arithmetic. To reduce 2000-bit data to 8 bits, $2000/8 = 250$ primes are needed. However, it is infeasible to find 250 co-prime integers within the 8-bit range $[0, 256)$. Consequently, precision reduction to 8-bit arithmetic involves two stages:

- (1) *Linear Precision Reduction*: RNS lowers high precision to an intermediate precision (e.g., 32-bit) with linear complexity.
- (2) *Quadratic Precision Reduction*: A secondary reduction further lowers the intermediate precision to 8-bit arithmetic, incurring quadratic complexity.

Table 1. Notations

Term	Conditions	Meaning (example value)
N	Power of two	Polynomial Degree (2^{16})
Q		Ciphertext modulus (1728 bits)
q_i	coprime	RNS base $Q = \prod_{i=0}^{L-1} q_i$ (28 bits)
L	$\log(Q)/\log(q_i)$	The number of limbs ($\lceil 1728/28 \rceil$ limbs)
$\log(q)$		RNS bases have $\log(q)$ bits
bp		bit precision of MAC in hardware
ω		a primitive $2N$ -th root of unity
$a_k \sim e_k$	$k \in [0, N-1]$	k -th degree coefficient of polynomial
$\mathbf{a} \sim \mathbf{e}$		coefficient vector
$dnum$		Number of digits in the switching key
\mathbf{m}		Original input message
$\llbracket \mathbf{m} \rrbracket$	$\llbracket \mathbf{m} \rrbracket = (P_{m1}, P_{m2})$	Ciphertext encrypting message \mathbf{m}
$\llbracket P_m \rrbracket_{q_i}$		q_i limb of P_m
P	$P = \prod_{j=1}^L p_j$	Auxiliary modulus
K		number of chunks
L'		number of limbs with auxiliary modulus
\mathcal{B}	$\mathcal{B} = q_0, \dots, q_{L-1}$	A set of RNS bases.
$(\mathbf{a})_{\mathcal{B}}$		coefficients vector under bases \mathcal{B}

2.1.3 Parameter Determination. The security level is determined by a pair of (degree N , ciphertext modulus bitwidth $\log_2(Q)$) for a given error standard deviation. Practical applications typically require 128-bit security level, which comes in various choices from $(2^{10}, 29)$ [5] to $(2^{17}, 2200+)$ [57]. A larger coefficient modulus ($\log_2(Q)$) allows more computation on a ciphertext before bootstrapping is required, but the degree N of the polynomial modulus must grow with $\log_2(Q)$ in order to maintain security. Larger Q and higher degree both lead to longer compute latency. Therefore, the minimal (degree, $\log_2(Q)$) that satisfies the required computation is often selected to minimize overheads.

2.2 HE Hardware Acceleration Requirements

In order to understand how prior works accelerate HE workloads and the performance limit of each candidate hardware, in this section, we first categorize the key challenges introduced by the HE workloads, followed by several speedup ingredients widely used by prior HE accelerators.

2.2.1 Challenges of HE Workloads. The overheads of HE are two-fold. First, HE encoding and encryption introduce about $200\times$ data expansion of the original message, making HE operators memory-bound for devices with small on-chip memory (*memory overhead*) [21, 34]. Second, evaluating encrypted data also introduces extra computation complexity, i.e. raw multiplication becomes ring polynomial multiplication in HE (*computation overhead*). Therefore, improving overall latency and efficiency boils down to reducing both off-chip data accesses and computation latency.

2.2.2 Key Hardware Speedup Ingredients. For both goals above, four key performance ingredients have been widely proposed in various compute platforms (Tab. 2).

- **High Clock Frequency:** It trades more power for low latency of computation and data movement.
- **High Parallelism:** HE workloads exhibit inherent parallelism due to the independence across ciphertexts, limbs and polynomial degree etc. Such independence brings high parallelism. For instance, under a 128-bit security parameter, a single raw-value multiplication necessitates at least $N = 2^{16}$ vectorized modular coefficient multiplications, all of which can be executed in parallel.
- **Large On-chip Memory:** HE workloads are often memory-bound [21, 34]. A sufficient on-chip memory caches commonly accessed data to reduce repeated data accesses from off-chip memory, saving critical latency.
- **Specialized Units:** HE operations are not natively supported in general-purpose hardware, leading to low performance mappings. For example, performing high-precision modular operations in HE using low-precision multipliers and adders on CPU or GPU are slow. A specialized modular reduction unit for selected category of modulus could deliver up to two order of magnitude speedup.

Further, HE operations such as NTT demonstrate static but different memory access patterns. The solutions are two-fold in prior works [3, 38, 39, 42, 53, 54]: (1) hardcode a dedicated hardware unit for each pattern, delivering significant performance improvement at cost of area and scheduling, (2) design an extra on-chip permutation unit that could support all required memory access patterns, e.g., transpose unit. Both deliver better performance and efficiency by non-consecutive access patterns into contiguous ones.

2.2.3 HE ASIC Accelerators. Examining CraterLake [54] as a representative HE ASIC accelerator, it showcases several features that enhance HE processing efficiency:

- **Freq.:** CraterLake operates at a 1 GHz clock frequency, which is $3.33\times$ higher than that of typical FPGA accelerators with dedicated architecture for HE operations.
- **High Parallelism:** It includes dedicated hardware components for HE operators, to offer an overall throughput of 165888 parallel 28-bit ModMuls.
- **Large Memory:** With 256 MB on-chip memory, CraterLake can store up to 21 ciphertexts, facilitating high parallelism with minimal reliance on off-chip memory access.
- **Specialized Units:** It features a specialized network designed to perform fixed-size matrix transpositions, hiding explicit memory latency behind critical path.

Despite significant performance gains, the design and fabrication of specialized hardware require years of development and millions of dollars in capital expenditure. Moreover, the development of practical software toolchains to support such dedicated hardware further delays market readiness. These substantial investments in time and resources explain why no commercially available products exist as of now.

2.3 Potential of AI Accelerators for HE Workloads

This work demonstrates that AI accelerators (e.g. TPUv4) equipped with compilation support could bring an extra order of magnitude higher performance per watt to GPU/FPGA implementations based on following insights.

- **Large Compute Array (Parallelism):** Each MXU in AI accelerators is $32\times$ larger (e.g., 128×128 in TPUv4) than those in GPUs (typically 4×4). The larger size of MXUs increases on-chip data reuse within the two-dimensional computation arrays, enhancing throughput per watt. Moreover, a sea of 2048 SIMD ALUs, sharing the same regfiles with MXUs, further increase data reuse.
- **Large On-chip Memory:** AI accelerators feature large on-chip memory. For instance, a single Google TPU v4 chip has 160 MB of on-chip memory, including 128 MB CMEM and 32 MB VMEM array in Fig. 3, which is $20\times/4\times$ larger than the AMD MI100 / NVIDIA A100. This substantial on-chip capacity can accommodate entire ciphertexts, eliminating the need for repeated accesses to off-chip

Table 2. Acceleration techniques from various hardware, with key attributes that make AI accel. potential for HE in bold.

	Intel Xeon 9282	AMD 5950X	AMD MI100	NVIDIA A100	FAB [3]	CraterLake [54]	Google TPUv4 [31]	MTIA [24]
	CPU [30]	CPU [7]	GPU [6]	GPU [48]	FPGA	HE ASIC	AI ASIC	AI ASIC
Technology Node	Intel 14nm	TSMC 7nm	TSMC 7nm	TSMC 7nm	TSMC 7nm	14/12 nm	TSMC 7nm	TSMC 7nm
Clock Frequency (GHz)	2.6~3.8	2.9~5.1	1.502	1.095	0.3	1	1.05	0.8
Throughput (INT8 TFlops)	N/A	N/A	184.6	624	24.5 [10]	N/A	275	102.4
Power (W)	400	105	300	400	225	400	170	25
Throughput Per Watt	N/A	N/A	0.615	1.56	0.11	N/A	1.61	4.096
On-chip Memory (MB)	77	64	8	40	43	256	128+32	128
Specialized Unit	AVX512	AVX512	SMT	SMT	Modular; Flexible datapath	Modular; NTT; Transpose	Transpose	Transpose

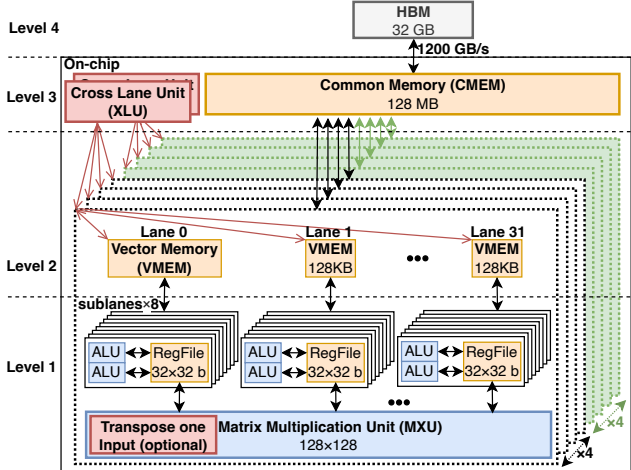


Figure 3. Overview of TPUv4 architecture based on public information [27, 31–33]. Four black dot boxes and four green dot boxes represent two tensor cores, separately. Two tensor cores share the same 128 MB common memory (CMEM). Each tensor core has 4 matrix multiplication units (MXU) and 2048 ALUs in Vector Processing Unit (VPU) organized as 128 SIMD lanes. Each lane consists of 8 SIMD sublanses with 128 KB vector memory (VMEM), each sublanses has 2 dual-issue ALUs and 128 B local register file. Each MXU features a 128×128 systolic array, and takes inputs from VMEMs. Each MXU is capable of performing matrix multiplication and each MXU has a local transpose unit to optionally transpose one input matrix in the pipelined manner to hide reordering latency behind. Data in VMEM of different lanes could get transposed or shuffled or reduced through the Cross Lane Unit (XLU), which consumes non-hidden layout reordering and reduction latency. The CMEM holds frequently used data to reduce off-chip memory accesses.

memory. By reducing off-chip memory traffic, it conserves bandwidth for fetching other necessary data and alleviates the memory bottlenecks inherent in HE workloads, leading to improved performance and efficiency.

- **Specialized Units:** AI ASICs consist of specialized on-chip transpose and permutation unit such as red Cross Lane Unit (XLU) in Fig. 3, which could be used to (1) permute or transpose data layout to convert strided on-chip memory access patterns into consecutive access patterns for less on-chip memory access latency, and (2) reduce data among multiple compute lanes.

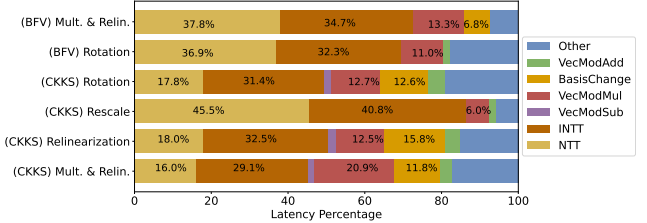


Figure 4. Latency profiling of HE Operators using OpenFHE, picking representative values for the parameters in Tab. 1. Vectorized Modular Multiplication (VecModMul), Addition (VecModAdd) and Subtraction (VecModSub) only count for latency not belonging to (I)NTT/Basis Change.

In summary, *large compute array, large on-chip memory and flexible permutation/transpose/reduction engine* in Tab. 2 enable AI accelerators to achieve better *performance per watt* in HE acceleration over existing CPU, GPU and FPGAs. However, effectively leveraging these abundant resources to accelerate HE remains a challenge due to the misalignment between computational patterns of HE workloads and architectural capabilities of AI accelerators.

The key of CROSS compiler framework is to convert high-precision modular HE workloads into low-precision convolution and matrix multiplication (GEMM) that could be efficiently processed on AI accelerators without any hardware modifications to achieve SotA performance per watt.

With this aim, we first characterize such misalignment and summarize key functional and performance challenges in §3. The key two ingredients of CROSS to bridge functional and performance misalignments, *Basis Align Transformation (BAT)* and *Matrix Align Transformation (MAT)* are then introduced in §4. Detailed analysis of using BAT and MAT for efficiently accelerating HE bottleneck operators, including NTT and BasisChange are introduced in §5, followed by an extensive evaluation, comparison to SotAs and conclusion.

3 Obstacles to Using AI Accelerator for HE

This section analyzes bottlenecks of HE operators and categorizes challenges of deploying them to AI accelerators.

3.1 Compute Patterns of Bottleneck HE Kernels

HE workloads fundamentally boil down to the scheduled invocation of essential HE operators, including HE Multiplication (Mult.), Relinearization (Relin.), Rotation, and Rescaling. In other words, the performance of these operators directly

determines the overall serving latency of HE workloads. To identify performance bottlenecks, we profiled various HE operators on an AMD Ryzen 9 5950X CPU with AVX support using OpenFHE library. The latency breakdown, presented in Fig. 4, reveals NTT, and its inverse (INTT), Basis Change, and Vectorized Modular Multiplication (VecModMul) and Addition (VecModAdd) are the five most time-consuming HE kernels in both CKKS and BFV schemes.

3.1.1 Number Theoretic Transform (NTT). The NTT converts polynomial representations from the coefficient domain to the evaluation domain, where polynomial multiplication simplifies to element-wise (vectorized) coefficient multiplication. The NTT and INTT are computationally intensive, accounting for approximately 45.1% to 86.3% of the overall latency in various HE operators.

The detailed algorithm is provided in Algorithm 1. In general, an N -point NTT consists of $\log_2(N)$ stages. Compute-wise, each stage comprises $\frac{N}{2}$ vectorized modular multiplications, additions, and subtractions, denoted as $\frac{N}{2}$ -VecModMul, $\frac{N}{2}$ -VecModAdd, and $\frac{N}{2}$ -VecModSub, respectively; Memory-wise, each stage also requires bit-complement shuffling [19].

Considering 8-point NTT depicted in Fig. 5a as an example, in stage 1, we perform a 4-element vectorized modular multiplication between $[a_4, a_5, a_6, a_7]$ and $[\omega, \omega^2, \omega^3, \omega^4]$:

$$[\tilde{a}_4, \tilde{a}_5, \tilde{a}_6, \tilde{a}_7] = [a_4 \cdot \omega, a_5 \cdot \omega^2, a_6 \cdot \omega^3, a_7 \cdot \omega^4] \pmod q$$

Then $vec = [a_0, a_1, a_2, a_3, \tilde{a}_4, \tilde{a}_5, \tilde{a}_6, \tilde{a}_7]$ is being reduced with the bit complement shuffled result of itself $vec = vec \pm \text{bit_complement_shuffle}(vec)$ using vectorized modular addition and subtraction to produce:

$$\begin{aligned} [b_0, b_1, b_2, b_3] &= [a_0 + \tilde{a}_4, a_1 + \tilde{a}_5, a_2 + \tilde{a}_6, a_3 + \tilde{a}_7] \pmod q \\ [b_4, b_5, b_6, b_7] &= [a_0 - \tilde{a}_4, a_1 - \tilde{a}_5, a_2 - \tilde{a}_6, a_3 - \tilde{a}_7] \pmod q \end{aligned}$$

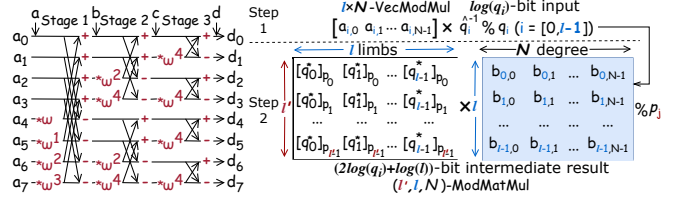
The bit-complement shuffling in the first stage has a group size of 8 elements [19], as illustrated by the permutation arrows in Fig. 5a. Subsequent stages perform the same bit-complement permutation with the group sizes decreasing by powers of 2 per stage.

Algorithm 1 Cooley-Tukey NTT [1]

Require: Coefficients set of input polynomial $P_m = (a_0, a_1, \dots, a_{N-1})$, N -th root of unity ω , total degree N .

Ensure: $NTT(P_m) = (b_0, b_1, \dots, b_{N-1})$

- 1: Initializes $b_i = a_i, i \in [0, N - 1]$; $\omega' = \omega$
 - 2: **for**($n = N, n > 1, n = n \gg 1$) ▷ Stage index
 - 3: $\omega_n = \omega^{\frac{N}{n}} \pmod q$
 - 4: **for**($i = 0, i < n, i = i + n$)
 - 5: **for**($j = 0, j < n, j = j + n$)
 - 6: $b[k+j] = (b[k+j] + \omega' b[k+j+n/2]) \pmod q$
 - 7: $b[k+j+n/2] = (b[k+j] - \omega' b[k+j+n/2]) \pmod q$
 - 8: $\omega' = \omega \cdot \omega_n \pmod q$
-



(a) 8-input NTT

(b) Basis Change

Figure 5. Illustration of computation patterns of NTT and Basis Change, superscript represents exponent.

3.1.2 Basis Change. Basis change is used to scale up or down polynomials in HE multiplication and rotation. An example of basis conversion from \mathcal{C} into \mathcal{B} is [16]:

$$\text{Conv}_{\mathcal{B}_1 \rightarrow \mathcal{B}_2}((a)_{\mathcal{B}_1}) = (\sum_{i=0}^{l'-1} [a_{n,i} \cdot \hat{q}_i^{-1}]_{q_i} \cdot [q_i^*]_{p_j} \pmod{p_j})_{0 \leq j < l', 0 \leq n < N}$$

where \hat{q}_i^{-1} and $[q_i^*]_{p_j}$ could be generated offline and get loaded into the on-chip memory as static parameters during runtime. During ModUp operation, $l = L/dnum$; $l' = K + (L - L/dnum)$, while in ModDown $l = K, l' = L$ (Tab. 1)

The above equation is broken into two steps (Fig. 5b).

- Step 1: $b_{n,i} = [a_{n,i} \cdot \hat{q}_i^{-1}]_{q_i}, 0 \leq i < l, 0 \leq n < N$ invokes l independent instances of N -length Vectorized Modular Multiplication, noted as $l \times N$ -VecModMul for simplicity.
- Step 2: $c_{n,j} = \sum_{i=0}^{l'-1} b_{n,i} \cdot [q_i^*]_{p_j} \pmod{p_j}, 0 \leq j < l', 0 \leq n < N$. It invokes one $M_{N \times l'} = M_{N \times l} \cdot M_{l \times l'}$ Modular Matrix Multiplication, noted as (N, l, l') -MatModMul.

3.2 Challenges of Accelerating HE on TPUv4

Table 3. HE computational patterns vs. AI accel. capabilities

	Primitive	Precision	Operation
HE	VecModAdd	$\log q$	$(a+b) \pmod q$
	VecModMul	$\log q$ ①	$(a \times b) \pmod q$
	ModMatMul	$\log q$ ②	$M_{H \times V} \cdot M_{V \times W} \pmod q$
	bit-complement shuffle	$\log q$	③ [19]
AI	VecAdd	(u)int32	$a+b$
AI	VecMul	(u)int32	$a \times b$
Accel.	MatMul	(u)int8	$M_{H \times V} \cdot M_{V \times W}$
TPUv4	Transpose	32 bit	$M_{H \times V} \rightarrow M_{V \times H}$
	Permutation	32 bit	Across Lane (Fig. 3)

①: $28 \leq \log q \leq 59$ under 128-bit security level; Intermediate results need $2 \log q$ bits, far exceeding precision range of typical AI accelerators.

②: intermediate results need $2 \log q + \log V$ bits to avoid overflow.

③: Bit complement negates the MSB of the binary representation of the index. Let s_i, d_i denote i -th bit of binary representation of a source and destination index of a value. Eg. after bit complement shuffling 8 elements, the 7-th value will go to the third location:

$$7 = \{s_2 = 1, s_1 = 1, s_0 = 1\} \rightarrow \{d_2 = \neg s_2, d_1 = s_1, d_0 = s_0\} = 3.$$

A comparison between the computational patterns of HE workloads and the capabilities of AI accelerators like TPUv4, as detailed in Table 3, reveals following *functional barriers*:

- **Lack of Native Modular Operations:** Neither the MXU nor VPU natively support modular reduction operations, which are fundamental to HE workloads.
- **Low-Precision Multipliers:** The MXU utilizes int8/bfloat16 multipliers with int32 adders, while the VPU operates

with FP32/int32 arithmetic. These low-precision units are insufficient for HE workloads with 28~59-bit post-RNS precision requirements.

Moreover, leveraging key architectural features of AI accelerator for HE presents additional *performance challenges*:

- **Memory Organization Constraints:** HE workloads are memory-bound, and misalignment between the bit-complement shuffling patterns required by NTTs and the transpose or permutation supported by AI accelerators increases the memory bandwidth requirements, exacerbating inefficiencies of memory boundness.
- **Parallelism Misalignment:** The parallelism in TPUv4 stems from its systolic array-based MXU, which is highly efficient for low-precision, large-scale dense matrix multiplication. However, most HE kernels, especially NTT, are inherently vectorized operations rather than matrix multiplications, leading to suboptimal MXU utilization.

Effectively addressing functional and performance gaps is crucial for enabling AI accel. to efficiently accelerate HE.

4 CROSS Compilation Framework

This section introduces how CROSS supports (1) scalar modular operation, (2) vectorized modular operations, and (3) modular matrix multiplication.

4.1 Enable Efficient High-precision Scalar Mod. Ops

HE has high-precision modular scalar multiplication, introducing two challenges for low-precision AI accelerators: (1) lack of modular reduction and (2) precision gap. This subsection introduces solutions separately.

4.1.1 Enable Modular Reduction as Multiplication.

CROSS adopts the Barrett modular reduction [12] to convert modular multiplication into two multiplications, one shifted multiplication, up-to two subtractions as signified in Alg. 2 with precision listed in comments. But these operations still deal with high-precision data.

Algorithm 2 Modular Multiplication and Barrett Reduction

Require: $a, b, m \in \mathbb{Z}_q$, $s = 2\lceil \log q \rceil$, $m = \lfloor 2^s/q \rfloor$.

Ensure: $z = a \cdot b \bmod q$

- 1: $z \leftarrow a \cdot b$ ▷ $\log q \times \log q \rightarrow 2 \log q$
 - 2: $t \leftarrow (z \cdot m) \gg s$ ▷ $2 \log q \times \log q \gg 2 \log q \rightarrow \log q$
 - 3: $z \leftarrow z - (t \cdot q)$ ▷ $2 \log q - \log q \times \log q \rightarrow 2 \log q$
 - 4: **if** $z \geq q$
 - 5: $z \leftarrow z - q$
-

4.1.2 Enable High-precision Ops using int8 MACs.

To resolve the precision gap, CROSS proposes *chunk-wise decomposition* to represent each high-precision coefficient as many low-precision chunks, such that high-precision arithmetic is achieved by many low-precision chunk-wise operations, as shown in Alg. 3, where HP indicates high-precision.

Algorithm 3 Chunk Decomposition: Map High-precision Scalar Operations as Low-precision Chunk-wise Operation

Require: $a, b, c \in \mathbb{Z}_q$ with $\log q$, $\log q$, $2 \log q$ bits, hardware bit precision bp , right shift s bits for shifted mul.

- 1: $K \leftarrow \lceil \frac{\log q}{bp} \rceil$ ▷ Number of chunks
 - 2: **procedure** CHUNKDECOMPOSE(a) $\rightarrow [a^k]_{0 \leq k < K}$
 - 3: $\text{bits} \leftarrow \text{binary}(a)$
 - 4: $a^k \leftarrow \text{bits}[k \cdot bp : (k+1) \cdot bp]$, for $0 \leq k < K$
 - 5: **end procedure**
 - 6: **procedure** CHUNKMERGE($[a^k]_{0 \leq k < K}$) $\rightarrow a$
 - 7: $a[k \cdot bp : (k+1) \cdot bp] = a^k$, for $0 \leq k < K-1$
 - 8: **end procedure**
 - 9: **procedure** CARRYPROPAGATE($[a^{k_1}]_{0 \leq k_1 < K}$) $\rightarrow [z^{k_2}]_{0 \leq k_2 < K+1}$ ▷ z has bp bits, a has larger than bp bits
 - 10: **for** iter in K :
 - 11: $\text{bits}^k \leftarrow \text{binary}(a^k)$; $\text{numbit}^k \leftarrow \text{len}(\text{bits}^k)$
 - 12: $a_L^k \leftarrow \text{numbit}^k[0 : \text{numbit}^k \gg -1]$;
 - 13: $a_H^k \leftarrow \text{bits}^k[\text{numbit}^k \gg : \text{numbit}^k - 1]$
 - 14: $z^0 = a_L^0$; $z^K = a_H^K$; $z^k = a_L^{k+1} + a_H^k$, $0 < k < K$
 - 15: $a^k = z^k$
 - 16: **end procedure**
 - 17: **procedure** HPSCALARADD(a, b) $\rightarrow z$ ▷ $z = a + b$
 - 18: $[a^k]_{0 \leq k < K} \leftarrow \text{CHUNKDECOMPOSE}(a)$
 - 19: $[b^k]_{0 \leq k < K} \leftarrow \text{CHUNKDECOMPOSE}(b)$
 - 20: $c^k = (a^k + b^k)$, for $0 \leq k < K$
 - 21: $z^k \leftarrow \text{CARRYPROPAGATION}(c^k)$, for $0 \leq k < K$
 - 22: $z \leftarrow \text{CHUNKMERGE}(z^k)$, for $0 \leq k < K$
 - 23: **end procedure**
 - 24: **procedure** HPSCALARMULT(a, b) $\rightarrow z$ ▷ $z = a \times b$
 - 25: $[a^k]_{0 \leq k < K} \leftarrow \text{CHUNKDECOMPOSE}(a)$
 - 26: $[b^k]_{0 \leq k < K} \leftarrow \text{CHUNKDECOMPOSE}(b)$
 - 27: $c^{k_1+k_2} += (a^{k_1} \times b^{k_2}) \cdot bp$, for $0 \leq k_1, k_2 < K$
 - 28: $z^k \leftarrow \text{CARRYPROPAGATION}(c^k)$, for $0 \leq k < 2K$
 - 29: $z \leftarrow \text{CHUNKMERGE}(z^k)$, for $0 \leq k < 2K$
 - 30: **end procedure**
 - 31: **procedure** HPSHIFTEDMULT(a, c) $\rightarrow z$ ▷ $z = a \times c \gg s$
 - 32: $a^k, c^k \leftarrow \text{CHUNKDECOMPOSE}(a, c)$
 - 33: $k_r = 0$ (k_r records the total number of right shifting)
 - 34: **for** $0 \leq k_z < \lceil \frac{3 \log q}{bp} \rceil$
 - 35: **for** $0 \leq k_1 \leq k_z$
 - 36: $z += (a^{k_1} \times c^{k_z-k_1}) \ll (k_z - k_r) \cdot bp$
 - 37: **if** $k_z < \lceil \frac{2 \log q}{bp} \rceil$
 - 38: $z = z \gg bp$ ▷ z is always using $\log q$ bits
 - 39: $k_r ++$
 - 40: **end procedure**
-

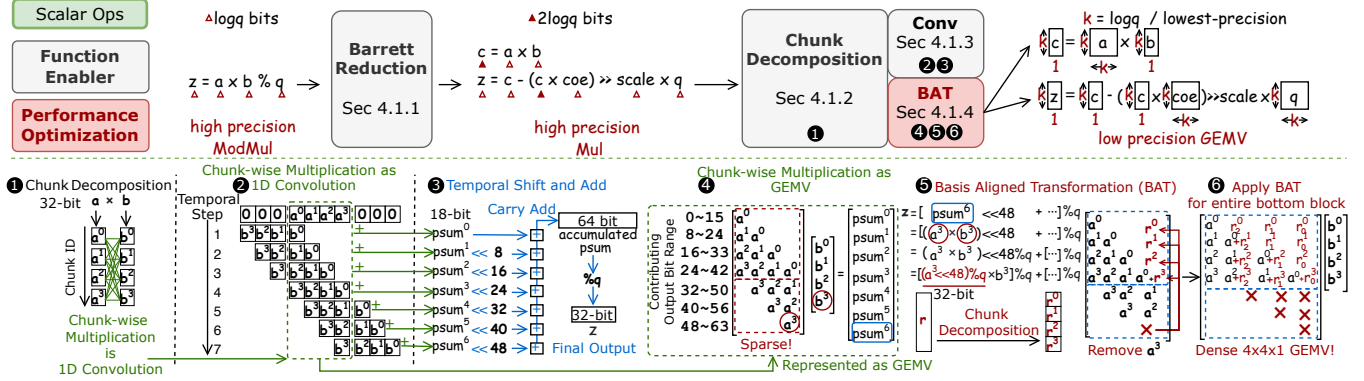


Figure 6. CROSS maps *high-precision scalar multiplication* into 1D convolution and temporal shifted accumulation (superscript represents chunk index). Further, Basis Align Transformation (**BAT**) further optimizes the 1D Convolution into a dense matrix vector multiplication (GEMV). Alternatively, BAT could convert b into matrix and a into vector.

Chunk Decomposition: Assuming the bit precision of hardware MAC is bp , a given data a with $\log q$ bits will be broken down into $K = \lceil \frac{\log q}{bp} \rceil$ chunks a^k , $0 \leq k < K$, each chunk has bp bits, as shown in Alg. 3. All high-precision data will be stored and computed as chunks.

High-precision Scalar Addition: A $\log q$ -bit addition boils down to (1) chunk decomposition, (2) chunk-wise addition, (3) carry propagation across chunks, and (4) bitwise concatenation to merge chunks back to the high-precision result.

High-precision Scalar Multiplication: Multiplying two $\log q$ -bit coefficients $a \times b$ to obtain a $2 \log q$ -bit result is mapped through (1) performing K^2 bp -bit multiplications for a^i, b^j , ($0 \leq i, j < K$), (2) shifted accumulation of chunk-wise multiplication results into final $2 \log q$ -bit result.

High-precision Shifted Scalar Multiplication: In Alg. 2, multiplying a $\log q$ -bit number by a $2 \log q$ -bit number produces a $3 \log q$ -bit result, which is ultimately right-shifted by $2 \log q$ bits to yield a $\log q$ -bit output. Therefore, the least significant $2 \log q$ bits serve only as temporary storage and need not be stored. To exploit this, CROSS partitions the $2 \log q$ -bit right shift into multiple steps, each discarding lower bp bits of the final result while accumulating chunk-wise multiplication product. As a result, this reduces $3 \log q$ -bit memory overhead of the final result to $\log q$ bits (Alg. 3).

Operations in Alg. 3 are only mapped to the VPU of TPUv4, which supports at most 32-bit integer arithmetic, i.e. $bp \leq 32$. Mapping Alg. 3 to MXU is inefficient because computation patterns does not fit the datapath of matrix multiplication engine, resulting in low utilization.

4.1.3 Schedule Chunk-wise Multiplication as Convolution. To leverage the available matrix multiplication engine of AI accelerators for accelerating chunk-wise multiplication, such as line 27 in Alg. 3, CROSS schedules low-precision chunk-wise multiplications as 1D convolution.

Taking mapping 32-bit coefficient multiplication to $bp = 8$ -bit compute as an example, as shown by ❶ in Fig. 6, CROSS

segments each coefficient into four uint8 chunks and then maps chunk-wise multiplication as 1D convolution (❷). Specifically, CROSS directly reads uint32 from local register, views it as a vector of four uint8 chunks, and pads $\frac{32}{bp} - 1 = 3$ zeros on both sides. Then, convolving the padded a with chunk-decomposed b over seven temporal cycles yields seven partial sums ($psum^k$, $k \in [0, 6]$), each at most $2bp + \log \frac{32}{bp} = 16 + 2 = 18$ bits². These partial sums are shifted and accumulated (❸) to 64-bit final result $psum$, which is stored in eight uint8 registers. $psum$ is finally modular reduced to 32 bits via Barrett Reduction (Alg. 2).

4.1.4 Basis Align Transformation (BAT). Although mapping chunk-wise multiplication as 1D convolution adapts its computation pattern to native datapath of the matrix multiplication engine in AI ASIC, in the chunk-wise multiplication example above, 3 padding zeros introduce 12 redundant computation, leading to an inefficiency of $16/(12 + 16) \approx 57\%$ effective compute utilization. To intuitively illustrate such an inefficiency, we represent such convolution-based mapping as matrix-vector multiplication as shown by ❹ in Fig. 6, where inefficiency is illustrated as zeros in the sparse left matrix. To remove such redundant computation, CROSS proposes BAT to convert the sparse matrix into a smaller dense matrix (❺), with detailed conversion introduced as follows.

In both the left matrix and its resulting vector (❹), elements in the same row contribute to the same bit range in the accumulated 64-bit partial sum $psum$. Specifically, for each row $k \in [0, 6]$, the contributed bit range is from $k \cdot bp$ to $(k + 2) \cdot bp + 2$. The minimal non-zero value contributed by each row is termed the row's *output basis*. For instance, the k -th row has an output basis of $2^{k \cdot bp}$.

Although the input left matrix spans seven distinct bases, after modular reduction, the final result z retains only the lowest four bases, corresponding to $k \in [0, 3]$. *All rows contributing to higher bases are intermediate results*. Hence, to

²Each each chunk-wise multiplication generates 16 bits. A reduction of $\frac{32}{bp} = 4$ chunks needs at most 2 extra bits to avoid precision overflow.

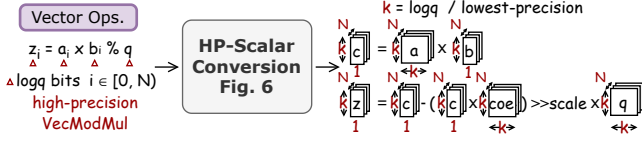


Figure 7. CROSS maps *vectorized modularized multiplication* (VecModMul) into low-precision GEMV.

remove elements associated with higher bases, CROSS applies a modular reduction step directly to those elements in the bottom blue dashed box of the left matrix (5), thereby *realigning* them with the four lowest bases and moving them back to the top blue dashed box (5 in Fig. 6). This process is thus termed as *Basis Align Transformation* (BAT).

For example, $a^3 \times b^3 = psum^6$ (in red circle of 4 and 5) illustrates BAT. $psum^6$, with the output basis of 2^{48} , is reduced to the four lowest bases in the final result. BAT applies the modular operator directly to $a^3 \ll 48$, yielding $r = (a^3 \ll 48) \bmod q$. The result, r , is 32 bits long and has a basis of 0. This allows chunk-wise decomposition to break r into four chunks (r^0, r^1, r^2, r^3) (5), which are then added back to the top dash box.

Applying BAT to all elements with bases higher than the final available bases converts the sparse input matrix into a smaller dense matrix (6), resulting in a $2\times$ computation speedup by halving the workload size. The transformed matrix will consume $\frac{\log q}{bp} \times$ memory than the original data, and thus BAT will be beneficial for compute-bound kernels, while Conv1D will still be invoked for memory-bound kernels.

At a higher level, BAT pays extra transformation overhead to eliminate redundant computation (5) and reduce the size of temporal reduction (4). Both improve computation efficiency. When value is pre-known, transformation overhead goes away because it happens offline.

4.2 Enable High-Precision Vectorized Modular Ops

Vectorized Modular Multiplication (VecModMul) with an arbitrary precision is mapped as a vector of high-precision scalar multiplication following Fig. 7, resulting in a depth-wise 1D convolution, where the degree is mapped as the convolution’s channel dimension. For performance speedup, if one vector in the operation is preknown, each 1D convolution could be converted into dense matrix-vector multiplication to reduce redundant compute.

Additionally, VecModMul with a modulus within 32 bits can leverage native 32-bit integer arithmetic directly on the VPU, further enhancing efficiency.

4.3 Enable High-Precision Matrix Modular Mul.

Although ModMatMul can be accelerated by the VPU via Barrett reduction, this mapping cannot leverage the inherent data reuse in MXU, leading to suboptimal efficiency. To address both precision and modular gaps while retaining data

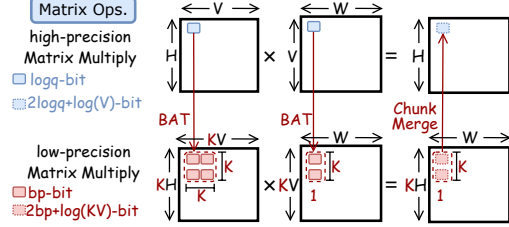


Figure 8. CROSS maps *high-precision matrix multiplication* into low-precision matrix multiplication with K times larger dimension to fully utilize MXU. $K = \lceil \frac{\log q}{bp} \rceil$ indicates the total number of chunks. Specifically, CROSS employs BAT to decompose each $\log q$ -bit element from the left and right matrices into a $K \times K$ array of bp -bit elements and a K -length vector. The data in resultant array have $2bp + \log(KV)$ bits to accommodate potential precision overflow during reduction. Note that BAT can also convert an element of the left matrix into a vector and an element of the right matrix into an array.

reuse for optimal performance, CROSS decomposes high-precision data into smaller chunks and reintegrates them into the original MatMul, forming a higher-dimensional MatMul. This approach bridges computational gaps and enhances utilization. An illustrative example is shown in Fig. 8.

In summary, this section introduces details of how CROSS supports various HE primitives including vectorized modular operators and modular matrix multiplication. This makes TPU an accelerator for HE under CROSS, because all HE kernels come as a combination of multiple primitives.

5 Apply CROSS to Accelerate HE on TPUv4

Enabling individual primitives facilitates HE acceleration on TPU. For better performance, this section introduces *inter-primitive optimizations* for NTT and BasisChange.

5.1 Case Study: Mapping NTT to MXU

5.1.1 Matrix Aligned Transformation (MAT). The standard Cooley-Tukey NTT for an input of size N performs $\log N$ rounds of operations—each round consisting of a vector modular multiplication (VecModMul), bit-complement shuffling, and vector modular addition (VecModAdd)³ (see §3.1.1). Although this method has a computational complexity of $O(N \log N)$, the bit-complement shuffling of N elements (with $N \geq 2^{16}$) introduces significant memory overhead. Large volumes of data must be transferred across VMEMs of multiple lanes via the XLU (refer to Fig. 3), which ultimately negates the computational savings.

To mitigate this issue, a 4-step NTT algorithm with $O(N\sqrt{N})$ complexity is commonly used on hardware with tensor cores [23, 26, 65]. As illustrated in Row 1 of Fig. 9, it consists of:

- Perform R -input NTTs on each of the C columns.

³ $N/2$ -VecModSub can be implemented as $N/2$ -VecModAdd using negated coefficients.

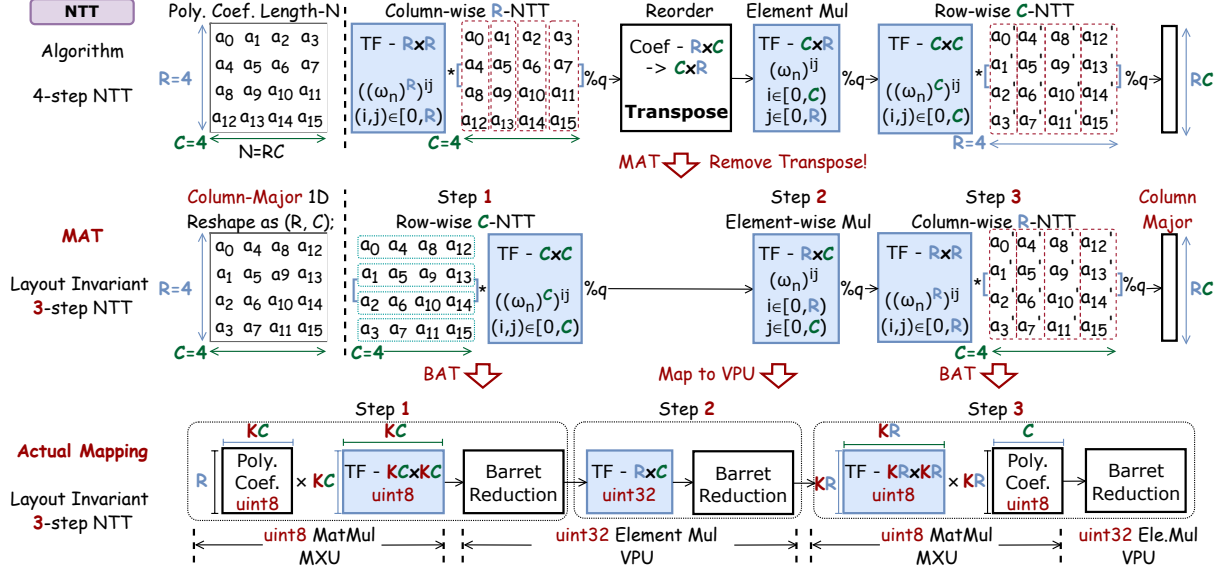


Figure 9. CROSS converts *high-precision NTT* into a combination of low-precision matrix multiplications and element-wise multiplications to fully exploit the MXU and VPU. Row 1 shows the conventional 4-step NTT algorithm [23]; Row 2 illustrates how the Matrix Aligned Transformation (MAT) eliminates the explicit transpose and keeps data layout invariant in NTT; Row 3 details the mapping of the MAT-optimized algorithm onto the TPU architecture. Here, TF denotes twiddle factor. Twiddle factors in step 1 and 3 become the same when $R = C$, such that only one TF matrix needs to be fetched and stored on-chip.

- Transpose resulting $R \times C$ matrix to obtain a $C \times R$ layout.
- Multiply by precomputed twiddle factors.
- Perform C -input NTTs on each of the R rows.

The need for an explicit transpose in 4-step NTT is costly. To eliminate it, we propose *MAT* with a *layout-invariant 3-step NTT*. In MAT, the 1D polynomial coefficients are stored in a column-major $R \times C^4$ matrix and the layout is unchanged throughout the NTT computation. By swapping the roles of the twiddle factor matrix and the input coefficient matrix in the step 1, the explicit transpose is avoided, yielding:

$$TF_{R \times R}^R @ \left[(a_{R \times C} @ TF_{C \times C}^C) \cdot TF_{C \times C} \right] \quad (1)$$

Here, the operator @ denotes matrix multiplication and \cdot represents element-wise multiplication. $TF_{R \times C}^k = \{(\omega^k)^{ij}\}, i \in [0, R], j \in [0, C], \omega$ is the primitive N -th root of unity. Note that $TF_{C \times C}^C$ is symmetric, i.e., $(TF_{C \times C}^C)^T = TF_{C \times C}^C$.

5.1.2 Mapping NTT to the TPU. In the layout-invariant 3-step NTT, the high-precision matrix multiplications in *steps 1 and 3* are converted by BAT into low-precision matrix multiplications, which are directly accelerated by the MXU.

For *modular reduction*, Barrett reduction is implemented as a vectorized operation and mapped to the VPU for SIMD-based parallel processing (see Alg. 2). Similarly, *element-wise multiplications* are mapped to the VPU following Fig. 7.

By combining MAT and BAT, our compiler efficiently maps NTT onto both the MXU and VPU. This approach achieves an effective computational complexity of $O(N\sqrt{N})$

⁴If the coefficients come as row-major, then we need to swap step 1 and 3 in Fig. 9.

Table 4. Challenges and Solutions

Challenge	CROSS Solution
No Modular Reduction	Barrett Reduction
Precision Gap	Chunk Decomposition
Inefficient Chunk-wise Ops.	Parallel Chunk-wise Ops. (BAT)
memory-costly 4-step NTT	Layout Invariant 3-step NTT (MAT)

while avoiding the memory-movement penalties associated with bit-complement shuffling. Consequently, the MAT-optimized NTT can yield up to a 1000× performance improvement over a purely vectorized NTT on TPUv4, which is particularly less performant under random data shuffling.

5.2 Case Study: Mapping Basis Change to MXU

For the *Basis Change* operation, our compiler employs a two-step mapping strategy. In Step 1 (see §3.1.2), the VPU accelerates the vector modular multiplication (VecModMul). In Step 2, which involves a (N, l, l') -sized matrix modular multiplication (MatModMul), the compiler uses both BAT and Barrett reduction to reformulate the operation as a higher-dimensional (KN, Kl, l') matrix multiplication, as shown in Fig. 8. This transformation allows the MXU to efficiently process the computation.

Under 128-bit security parameters, the dimensions Kl' and Kl typically range below but near 128. To maximize performance, the optimal block sizes are determined via an exhaustive brute-force search.

6 Evaluation

This section assesses TPUv4’s efficiency with other existing platforms. While TPUv4 with CROSS outperforms CPUs, GPU (V100+100x [34]), and FPGA (Xilinx Alveo U280+FAB [3]), it lags behind dedicated HE ASICs for lack of specialized units for bit-complement shuffling in NTT, not picking hardware-friendly moduli and less compute/memory. Additionally, we explore the performance improvement and overhead of integrating dedicated modular components.

6.1 Methodology

We select Google’s TPU as a representative ASIC AI accelerator and enable deployment on a real TPUv4 by converting HE kernels into convolution and MatMul and leveraging JAX [14] and Pallas [9] to program TPUv4. We report the latency from trace_viewer in XLA profiler [18].

Security Parameter Setup The 128-bit security is commonly accepted security level and Tab. 6 lists 6 potential parameter setups with different post-RNS precision. Lower post-RNS precision always gives better performance on TPUv4. This is because processing larger bitwidth data in the MXU’s low-precision MAC leads to a quadratic increase in the total number of chunk-wise multiplication, as explained in §2.1.2. Therefore, we choose security parameter set 6 with 28-bit modular precision throughout the the evaluation.

CROSS Configurations For security parameter set 6, each 28-bit coefficient is stored in 32-bit unsigned integer and decomposed into $K = \lceil \frac{\log q=28}{bp=8} \rceil = 4$ chunks if leveraging MXU. Further, CROSS configures layout invariant 3-step NTT with 2^8 -NTT in both step 1 and step 3. Eg. step 1 is finally converted to $(R, KC, KC)=(256, 1024, 1024)$ 8-bit MatMul with each element stored as unsigned 8-bit integer. Note that all twiddle factors are compiled offline and prefetched to TPU, consuming 1.25 MB on-chip memory. To achieve apple-to-apple comparison with other works, we pick 128 as the batch size throughout the evaluation. We note that CROSS is more performant when setting batch size as higher value and utilizing a cluster of multiple TPU chips.

Baseline Performance is highly dependent on security parameters, we adopt each platform’s published configurations when evaluating the same HE operators. Specifically, CPU: (1) OpenFHE running on an AMD 5950× with AVX-512 and multithreading (2) State-of-the-art Lattigo [47] running on an Intel i5-6600k with AVX2; GPU: (1) 100× [34] on an NVIDIA V100; (2) TensorFHE [23] on an NVIDIA A100; (3) Cheddar [37] on an NVIDIA A100; FPGA: SotA FAB [3]. Wall-clock latencies for GPUs and FPGA are taken directly from their respective publications [3, 34]. We also compare against various SotA HE ASICs and select CraterLake [54] as our ASIC baseline because its setup aligns with CROSS. To enable fair comparison with Google TPUv4, we proportionally scale CraterLake’s compute and memory resources

Table 5. Logistic Regression comparison with HE ASICs. Speedup of CROSS over other designs is in bold, unit: ms.

hardware	Sharp	BTS	ARK	CL [54]	CROSS
Type					
	HE ASIC				AI ASIC
Power (W)	178.8	163.2	281.3	170	170
Security level	128	128	128	128	128
Logistic Regression	2.53	28.4	14.3	15.2	83.98

to achieve comparable power. An overview of different baselines is detailed in Tab. 6.

Workload: We adopt ML workloads without bootstrapping including LoLa-MNIST, LeNet and Logistic Regression⁵ [29], and four backbone HE kernels as workloads, including HEAdd, HEMult, HERescale and HERotate [17]. Such kernel-wise comparisons show its generality on various applications.

6.2 Comparison against SotAs

SotAs on Available Devices: CROSS enables TPUv4 to achieve (1) 327× and 12× speedup over OpenFHE (AMD 5950, CPU) and SoTA Lattigo (Intel i5-6600k, CPU), (2) 5× speedup over NVIDIA-V100 (100× [34]) and 0.5× slower than SotA NVIDIA-A100 (Cheddar [37]), (3) 1.05× speedup SotA FPGA (Xilinx Alveo U280 + FAB [3]), as shown in the Tab. 6. We note that NVIDIA-A100 has 2.35× more power consumption so that TPUv4 achieves 1.17× better performance per watt over NVIDIA-A100 + Cheddar [37]. Further, under one simple LeNet-style network, LoLa-MNIST, tested on the MNIST dataset [15], TPU with CROSS consumes 49 ms for a single inference, which is 60× faster than OpenFHE (AMD 5950, CPU). This is because, by effectively leveraging available compute and memory from TPUv4 via CROSS, the overall throughput is significantly larger than that of CPU.

HE ASIC SotA: Under Logistic Regression as the workload, compared against HE ASIC accelerators such as Sharp [38], CraterLake [54], ARK [39] and BTS [41], TPUv4 with CROSS is 33.2×/2.96×/5.87×/5.53× slower, which is derived from the HE-Mult slowdown in Tab. 6 for lack of dedicated hardware for modular operations and NTT.

NTT Throughput Comparison: NTT is the dominant latency kernel in HE serving, so accelerating NTT directly improves overall performance. Under HEAX parameter sets A, B, and C (Tab. 2 in [52]) with polynomial degrees of 2^{12} , 2^{13} , and 2^{14} , TPUv5p, TPUv6, TPUv5e, and TPUv4 achieve speedups of up to 26×, 23×, 13×, and 7× over HEAX, respectively. In addition, our design outperforms FAB (Xilinx U280 FPGA) by 6.3×, 5.7×, 3.2×, and 1.9×, and TensorFHE (A100 GPU) by 4.8×, 3.7×, 2.5×, and 1.5× (see Fig. 11a). This performance gain is attributed to two key optimizations in CROSS’s implementation of outer-product, chunk-wise multiplication in TensorFHE:

⁵HELR [28] is a binary classification model using logistic regression. We trained the model for 32 iterations, each with a batch containing 1024 14×14-pixel MNIST images, where an iteration is a gradient update step with a single batch, and report average execution time per iteration.

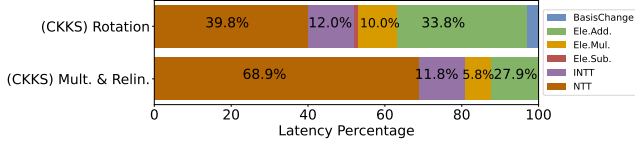


Figure 10. Latency profiling of latency-dominating kernel including HE multiplication and HE rotation on TPUv4, picking security parameter set 6 from Tab. 6.

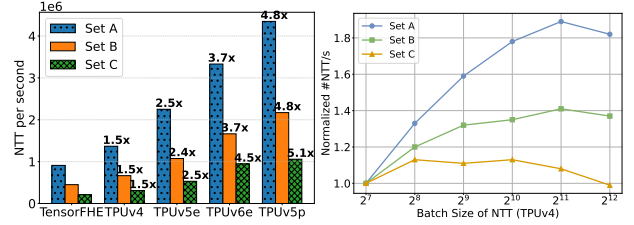
- *BAT* reduces the size of intermediate results to N , thereby reducing memory consumption of intermediate results. The detailed algorithm for a 28-bit modulus is presented in Alg. 4.
- *In-place Chunk Decomposition*: By compiling the chunk decomposition as an alternative parsing of the input data—without explicit data movement—and stacking decomposed chunks into larger matrices for GEMM operations, compute utilization is significantly improved.

Performance Deep Dive: Under security set 6, Fig. 10 shows the latency breakdown of the two dominant kernels, HE-Mult and HE-Rotate. In HE-Mult, NTT and INTT account for 68% and 5.8% of the total latency, respectively, while in HE-Rotate they contribute 39.8% and 10%. Moreover, the Basis Change operation consumes 27.9% of latency in HE-Mult and 33.8% in HE-Rotate due to low arithmetic reuse. As both kernels are memory-bound, these results highlight the potential benefits of further memory compression and optimization techniques.

6.3 Ablation Study

6.3.1 Impact of Workload Sizes. MatMul in HE workloads mainly arises from NTT and BasisChange operations. NTT-based MatMul typically involves square matrices of size 2^7 to 2^{10} , whereas BasisChange results in skewed MatMul, with one dimension equal to degree N and the other being the number of limbs l or l' . We evaluated the performance of the proposed precision reduction techniques, BAT and convolution-based mapping (Fig. 6), with latency metrics for various sizes (Tab. 7). The latency of MAT + BAT scales roughly linearly with the increase in FLOPs, achieving approximately 85% computation utilization on average. Additionally, BAT consistently improves performance by 1.08× to 1.99× over convolution-based mapping, owing to reduced redundant zero computation and less temporal reductions.

6.3.2 Impact of Batch Size. As shown in Fig. 11b, increasing the batch size improves NTT throughput on the TPU (normalized relative to a batch size of 128). Larger batches enable multiple ciphertexts to reuse the same twiddle factors, which reduces redundant off-chip memory accesses and increases operational intensity—shifting the workload from being compute-bound toward a more efficient memory-bound regime. However, when the batch size is too high, input coefficients kicks twiddle factors of the three NTT



(a) NTT/s vs TensorFHE-A100.

(b) Batch Size.

Figure 11. Ablation study: Impact of Different Hardware and Batch Size on NTT Throughput.

stages out from on-chip memory, leading to repeated off-chip loads and degraded performance. Increasing on-chip memory capacity would alleviate this bottleneck and further enhance throughput.

6.3.3 BAT vs. Conv. We evaluate the performance of Batched Aggregated Transformation (BAT) against conventional convolution (Conv) for matrix multiplications in NTT and Basis Change (see Tab. 7). Both BAT and Conv achieve significant speedup than temporal chunk-wise multiplication. BAT delivers up to a 1.99× higher speedup over Conv, because matrix multiplication converted from NTT and basis change are compute bound by nature, so that transforming the sparse GEMM operations used in Conv into dense matrix multiplications, reducing overall Flops.

6.3.4 Betterfly NTT vs. MAT NTT. MAT does increase $O(N \log N)$ butterfly NTT into $O(N\sqrt{N})$, and it brings up-to 6-magnitude speedup over butterfly NTT on TPU, as shown in Tab. 8, because shuffling index needs to be compiled offline and get fetched to the compute during runtime, worsening memory boundness and introducing extra run-time data shuffling latency. MAT eliminates such memory and run-time shuffling overhead by converting it into ModMatMul.

6.3.5 BasisChange w/ BAT vs. w/o BAT. When the reduction dimension in MatMul is not divisible by 128, CROSS pads zeros, leading to partial MXU utilization for the last tile. To address this, CROSS leverages BAT: Stacks k^2 8-bit (l', l, N) -ModMatMul operations into a single larger (kl', kl, N) -ModMatMul, increasing utilization and achieving up-to 8.73× speedup, as shown in Tab. 9.

6.4 Performance Gap to Dedicated FHE ASICs

The performance gap between CROSS on TPU and dedicated FHE ASICs is driven by three factors:

- **Hardware-Friendly Moduli:** Dedicated FHE ASICs [53, 54] use fixed moduli (e.g., $2^{32} - v$, with v as a 16-bit value) optimized for hardware. In contrast, CROSS supports arbitrary moduli, which can incur a 2~3× performance penalty depending on the implementation. Notably, CROSS can be configured to use hardware-friendly moduli as well, which we leave as future efforts.

Table 6. HE kernel latency comparison with SotAs. Speedup of CROSS over other designs is in bold, unit: *us*. Speedup or slowdown of CROSS on TPU compared to SotAs are listed in parenthesis, unavailable data is noted as N/A.

Library	OpenFHE [11]	Lattigo [47]	100x[34]	Cheddar [37]	FAB [3]	CraterLake [54]	CROSS
hardware	AMD 5950	i5-6600k	V100	A100	Alevo U280	Dedicated	TPUv4
Type	CPU	CPU	GPU	GPU	FPGA	HE ASIC	AI ASIC
Power (W)	105	65	300	400	215	170	170
Technology Node	7 nm	14 nm	12 nm	7 nm	16 nm	14/12 nm	7 nm
Date Introduced	2020	2015	2017	2020	2019	2022	2021
Parameter Setup	Set 1	Set 2	Set 3	Set 4	Set 5	Set 6	
($\log PQ, \log Q, \log(q)^*$)	(2596, 1947, 59)	(1728, N/A, N/A)	(3220, 2305, 52)	(1767, N/A, 52)	(2364, 1693, 52)	(1904, 1428, 28)	
Degree (N), Limb (L)	(2^{17} , 33)	(2^{16} , 31)	(2^{17} , 44)	(2^{16} , 54)	(2^{16} , 32)	(2 ¹⁶ , 51)	
D_{num}	3		3	3	4	3	3
Security level	128	128	128	128	128	128	128
Ciphertext Size (MB)	60.84	N/A	35.75	N/A	13	11.15	
HE-Add (Latency, us)	31423 (730×)	4500 (104.7×)	378 (8.8×)	80 (2.5×)	40 (0.93×)	8.75 (0.2×)	43
HE-Mult (Latency, us)	533497 (327×)	19400 (12×)	7960 (5×)	850 (0.5 ↓)	1710 (1.05×)	35 (0.02 ↓)	1628
Rescale (Latency, us)	5784 (26.8×)	65700 (304×)	1200 (5.56×)	N/A	190 (0.88 ↓)	9 (0.04 ↓)	216
Rotate (Latency, us)	442224 (392×)	N/A	6600 (5.85×)	N/A	1570 (1.39×)	27 (0.02 ↓)	1128

Table 7. BAT vs. Convolution on $M_{H \times V} \cdot M_{V \times W} \bmod q$

	H	V	W	MAT+Conv.	MAT+BAT	speedup
NTT range	256	256	256	49.36 μs	24.83 μs	1.99×
	512	512	512	52.03 μs	42.11 μs	1.24×
	512	1024	1024	136.76 μs	124.38 μs	1.10×
	2048	2048	2048	2 ms	1.36 ms	1.50×
Basis Change	16384	256	256	429.40 μs	345.90 μs	1.24×
	16384	1024	256	1,118.35 μs	806.75 μs	1.39×

Table 8. Performance Comparison of Butterfly NTT and MAT-based NTT on TPUv4 (unit: us). OOM: out-of-memory. Degree $N = R \times C$

Degree	R	C	butterfly NTT	MAT NTT	Speedup
2 ¹³	128	64	111098	0.92	120758×
2 ¹⁴	128	128	505248	3.45	146448×
2 ¹⁵	256	128	2101739	6.90	304599×
2 ¹⁶	256	128	OOM	16.47	$\infty \times$

Table 9. Performance of BasisChange w/ and w/o BAT

limb_in	limb_out	Degree	No-BAT	BAT	Speedup
12	28	65536	364.31	85.42	4.26×
12	36	65536	698.05	96.73	7.22×
16	40	65536	839.83	96.16	8.73×
20	48	65536	838.52	106.38	7.88×
24	56	65536	768.10	121.21	6.34×

- **Low-Cost All-to-All Shuffling:** Dedicated accelerators feature efficient shuffling mechanisms—such as the layout transpose unit in CraterLake [54] and the all-to-all connected NoC in FAB [3]—that enable a butterfly recursive NTT with $O(N \log N)$ complexity. This design choice yields up to a 16× performance advantage than layout invariant 3-step NTT with $O(N\sqrt{N})$ compute complexity when picking polynomial degree $N = 2^{16}$.
- **Extensive Compute and Large On-Chip Memory:** Dedicated FHE ASICs allocate a significant portion of chip area to on-chip memory (e.g., a 256 MB on-chip memory, double of TPUv4), which supports larger batch sizes and increased data reuse, thereby enhancing overall performance.

Three factors accumulated explain the 32× and 50× performance gap listed in Tab. 5 and Tab. 6.

7 Related Work

Previous studies on hardware-accelerated HE follow two main tracks. The first track proposes custom ASIC designs with the sole purpose of accelerating HE workloads. Initial proposals were relatively small [53] but quickly grew to chips requiring hundreds of MB in memory and hundreds of mm² in area [42, 54, 57]. While these designs achieve significant performance gains over CPU baselines, they would cost millions of dollars to fabricate and deploy.

This motivates the second track of prior works, which use existing hardware to accelerate HE workloads. Following the path of AI acceleration, these works focus on GPU acceleration [22, 23, 34, 37, 40, 44, 57, 58, 64] as well as employing FPGAs as more configurable commodity hardware [3, 52, 60]. Our work falls into this second category, proposing a novel compilation techniques to better utilize *existing* hardware to accelerate HE workloads at no additional hardware cost. With the first trail [35] directly maps polynomial multiplication as matrix multiplication, this work continues the path of adapting AI accelerators for HE workloads as a promising platform for HE. This work shows that TPUv4 can be competitive with GPUs and FPGAs, enabling the same chip to support both privacy-preserving AI and raw AI. Further studies are required to support bootstrapping.

8 Conclusion

This work demonstrates the potential of AI accelerators (such as Google TPUv4) to accelerate Homomorphic Encryption workloads, offering competitive performance compared to CPU, SotA GPU, and SotA FPGA alternatives. We introduced CROSS, a compilation framework that enhances HE processing on TPU. CROSS is the first work enabling both AI and HE serving at the price of fabricating only one chip, enabling immediate privacy-preserving serving without significant time and money costs. We leave bootstrapping and inter-kernel optimizations as future work.

References

- [1] R.C. Agarwal and C.S. Burrus. Number theoretic transforms to implement fast digital convolution. *Proceedings of the IEEE*, 63(4):550–560, 1975.
- [2] Rashmi Agrawal, Leo de Castro, Chiraag Juvekar, Anantha Chandrakasan, Vinod Vaikuntanathan, and Ajay Joshi. Mad: Memory-aware design techniques for accelerating fully homomorphic encryption. 2023.
- [3] Rashmi Agrawal, Leo de Castro, Guowei Yang, Chiraag Juvekar, Rabia Yazicigil, Anantha Chandrakasan, Vinod Vaikuntanathan, and Ajay Joshi. Fab: An fpga-based accelerator for bootstrappable fully homomorphic encryption, 2022.
- [4] Ahmad Al Badawi, Yuriy Polyakov, Khin Mi Mi Aung, Bharadwaj Veeravalli, and Kurt Rohloff. Implementation and performance evaluation of rns variants of the bfv homomorphic encryption scheme. *IEEE Transactions on Emerging Topics in Computing*, 9(2):941–956, 2021.
- [5] Martin Albrecht, Melissa Chase, Hao Chen, Jintai Ding, Shafi Goldwasser, Sergey Gorbunov, Shai Halevi, Jeffrey Hoffstein, Kim Laine, Kristin Lauter, et al. Homomorphic encryption standard. *Protecting privacy through homomorphic encryption*, pages 31–62, 2021.
- [6] AMD. Amd mi100 specifications, 2023.
- [7] AMD. Amd ryzen™ threadripper™ 7980x specifications, 2023.
- [8] Yongdae An, Seungmyung Lee, Seungwoo Jung, Howard Park, Yongsoo Song, and Taehoon Ko. Privacy-oriented technique for covid-19 contact tracing (protect) using homomorphic encryption: Design and development study. *J Med Internet Res*, 23(7):e26371, Jul 2021.
- [9] JAX authors. Pallas: a jax kernel language, 2024.
- [10] Avent. Alveo series performance on ml inference, 2024.
- [11] Ahmad Al Badawi, Jack Bates, Flavio Bergamaschi, David Bruce Cousins, Saroja Erabelli, Nicholas Genise, Shai Halevi, Hamish Hunt, Andrey Kim, Yongwoo Lee, Zeyu Liu, Daniele Micciancio, Ian Quah, Yuriy Polyakov, Saraswathy R.V., Kurt Rohloff, Jonathan Saylor, Dmitriy Suponitsky, Matthew Triplett, Vinod Vaikuntanathan, and Vincent Zucca. Openfhe: Open-source fully homomorphic encryption library. Cryptology ePrint Archive, Paper 2022/915, 2022. <https://eprint.iacr.org/2022/915>.
- [12] Paul Barrett. Implementing the rivest shamir and adleman public key encryption algorithm on a standard digital signal processor. In *Proceedings on Advances in Cryptology—CRYPTO ’86*, page 311–323, Berlin, Heidelberg, 1987. Springer-Verlag.
- [13] Fabian Boemer, Sejun Kim, Gelila Seifu, Fillipe DM de Souza, Vinodh Gopal, et al. Intel HEXL (release 1.2). <https://github.com/intel/hexl>, 2021.
- [14] James Bradbury, Roy Frostig, Peter Hawkins, Matthew James Johnson, Chris Leary, Dougal Maclaurin, George Necula, Adam Paszke, Jake VanderPlas, Skye Wanderman-Milne, and Qiao Zhang. JAX: composable transformations of Python+NumPy programs, 2018.
- [15] Alon Brutzkus, Oren Elisha, and Ran Gilad-Bachrach. Low latency privacy preserving inference, 2019.
- [16] Jung Hee Cheon, Kyoohyung Han, Andrey Kim, Miran Kim, and Yongsoo Song. A full rns variant of approximate homomorphic encryption. In *Selected Areas in Cryptography—SAC 2018: 25th International Conference, Calgary, AB, Canada, August 15–17, 2018, Revised Selected Papers 25*, pages 347–368. Springer, 2019.
- [17] Jung Hee Cheon, Andrey Kim, Miran Kim, and Yongsoo Song. Homomorphic encryption for arithmetic of approximate numbers. Cryptology ePrint Archive, Paper 2016/421, 2016. <https://eprint.iacr.org/2016/421>.
- [18] Google Cloud. Profile your model on cloud tpu nodes, 2024.
- [19] William James Dally and Brian Patrick Towles. *Principles and practices of interconnection networks*. Elsevier, 2004.
- [20] Roshan Dathathri, Olli Saarikivi, Hao Chen, Kim Laine, Kristin Lauter, Saeed Maleki, Madanlal Musuvathi, and Todd Mytkowicz. Chet: Compiler and runtime for homomorphic evaluation of tensor programs, 2018.
- [21] Leo de Castro, Rashmi Agrawal, Rabia Yazicigil, Anantha Chandrakasan, Vinod Vaikuntanathan, Chiraag Juvekar, and Ajay Joshi. Does fully homomorphic encryption need compute acceleration?, 2021.
- [22] Guang Fan, Fangyu Zheng, Lipeng Wan, Lili Gao, Yuan Zhao, Jiankui Dong, Yixuan Song, Yuewu Wang, and Jingqiang Lin. Towards faster fully homomorphic encryption implementation with integer and floating-point computing power of gpus. In *2023 IEEE International Parallel and Distributed Processing Symposium (IPDPS)*, pages 798–808, 2023.
- [23] Shengyu Fan, Zhiwei Wang, Weizhi Xu, Rui Hou, Dan Meng, and Mingzhe Zhang. Tensorfhe: Achieving practical computation on encrypted data using gpgpu, 2022.
- [24] Amin Firoozshahian, Joel Coburn, Roman Levenstein, Rakesh Nattoji, Ashwin Kamath, Olivia Wu, Gurdeepak Grewal, Harish Aepala, Bhaskar Jakka, Bob Dreyer, Adam Hutchin, Utku Diril, Krishnakumar Nair, Ehsan K. Aredestani, Martin Schatz, Yuchen Hao, Rakesh Komuravelli, Kunming Ho, Sameer Abu Asal, Joe Shajrawi, Kevin Quinn, Nagesh Sreedhara, Pankaj Kansal, Willie Wei, Dheepak Jayaraman, Linda Cheng, Pritam Chopda, Eric Wang, Ajay Bikumandla, Arun Karthik Sengottuvel, Krishna Thottempudi, Ashwin Narasimha, Brian Dodds, Cao Gao, Jiyuan Zhang, Mohammed Al-Sanabani, Ana Zethabioskuie, Jordan Fix, Hangchen Yu, Richard Li, Kaustubh Gondkar, Jack Montgomery, Mike Tsai, Saritha Dwarakapuram, Sanjay Desai, Nili Avidan, Poorvaja Ramani, Karthik Narayanan, Ajit Mathews, Sethu Gopal, Maxim Naumov, Vijay Rao, Krishna Noru, Harikrishna Reddy, Prahlad Venkatapuram, and Alexis Bjorlin. Mtia: First generation silicon targeting meta’s recommendation systems. In *Proceedings of the 50th Annual International Symposium on Computer Architecture, ISCA ’23*, New York, NY, USA, 2023. Association for Computing Machinery.
- [25] Xinwei Fu, Zhen Zhang, Haozheng Fan, Guangtai Huang, Randy Huang, Rahul Solanki, Fei Wu, Ron Diamant, and Yida Wang. Distributed training of large language models on aws tranium. 2024.
- [26] W Morven Gentleman and Gordon Sande. Fast fourier transforms: for fun and profit. In *Proceedings of the November 7-10, 1966, fall joint computer conference*, pages 563–578, 1966.
- [27] Google. Google Cloud TPU, 2024.
- [28] Kyoohyung Han, Seungwan Hong, Jung Hee Cheon, and Daejun Park. Logistic regression on homomorphic encrypted data at scale. In *Proceedings of the AAAI conference on artificial intelligence*, volume 33, pages 9466–9471, 2019.
- [29] Kyoohyung Han, Seungwan Hong, Jung Hee Cheon, and Daejun Park. Logistic regression on homomorphic encrypted data at scale. In *Proceedings of the Thirty-Third AAAI Conference on Artificial Intelligence and Thirty-First Innovative Applications of Artificial Intelligence Conference and Ninth AAAI Symposium on Educational Advances in Artificial Intelligence, AAAI’19/IAAI’19/EAAI’19*. AAAI Press, 2019.
- [30] Intel. Intel® xeon® platinum 9282 processor specifications, 2023.
- [31] Norman P. Jouppi, Doe Hyun Yoon, Matthew Ashcraft, Mark Gottscho, Thomas B. Jablin, George Kurian, James Laudon, Sheng Li, Peter Ma, Xiaoyu Ma, Thomas Norrie, Nishant Patil, Sushma Prasad, Cliff Young, Zongwei Zhou, and David Patterson. Ten lessons from three generations shaped google’s tpuv4i : Industrial product. In *2021 ACM/IEEE 48th Annual International Symposium on Computer Architecture (ISCA)*, pages 1–14, 2021.
- [32] Norman P. Jouppi, George Kurian, Sheng Li, Peter Ma, Rahul Nagaranjan, Lifeng Nai, Nishant Patil, Suvinay Subramanian, Andy Swing, Brian Towles, Cliff Young, Xiang Zhou, Zongwei Zhou, and David Patterson. Tpu v4: An optically reconfigurable supercomputer for machine learning with hardware support for embeddings, 2023.

- [33] Norman P. Jouppi, Doe Hyun Yoon, George Kurian, Sheng Li, Nishant Patil, James Laudon, Cliff Young, and David A. Patterson. A domain-specific supercomputer for training deep neural networks. *Commun. ACM*, 63(7):67–78, 2020.
- [34] Wonkyung Jung, Sangpyo Kim, Jung Ho Ahn, Jung Hee Cheon, and Younho Lee. Over 100x faster bootstrapping in fully homomorphic encryption through memory-centric optimization with gpus. *IACR Transactions on Cryptographic Hardware and Embedded Systems*, pages 114–148, 2021.
- [35] Rabimba Karanjai, Sangwon Shin, Wujie Xiong, Xinxin Fan, Lin Chen, Tianwei Zhang, Taeweon Suh, Weidong Shi, Veronika Kuchta, Francesco Sica, and Lei Xu. Tpu as cryptographic accelerator. In *Proceedings of the International Workshop on Hardware and Architectural Support for Security and Privacy 2024*, HASP '24, page 37–44, New York, NY, USA, 2024. Association for Computing Machinery.
- [36] Jongmin Kim, Wonseok Choi, and Jung Ho Ahn. Cheddar: A swift fully homomorphic encryption library for cuda gpus, 2024.
- [37] Jongmin Kim, Wonseok Choi, and Jung Ho Ahn. Cheddar: A swift fully homomorphic encryption library for cuda gpus. *arXiv preprint arXiv:2407.13055*, 2024.
- [38] Jongmin Kim, Sangpyo Kim, Jaewan Choi, Jaiyoung Park, Donghwan Kim, and Jung Ho Ahn. Sharp: A short-word hierarchical accelerator for robust and practical fully homomorphic encryption. In *Proceedings of the 50th Annual International Symposium on Computer Architecture*, ISCA '23, New York, NY, USA, 2023. Association for Computing Machinery.
- [39] Jongmin Kim, Gwangho Lee, Sangpyo Kim, Gina Sohn, Minsoo Rhu, John Kim, and Jung Ho Ahn. Ark: Fully homomorphic encryption accelerator with runtime data generation and inter-operation key reuse. In *2022 55th IEEE/ACM International Symposium on Microarchitecture (MICRO)*, pages 1237–1254, 2022.
- [40] Sangpyo Kim, Wonkyung Jung, Jaiyoung Park, and Jung Ho Ahn. Accelerating number theoretic transformations for bootstrappable homomorphic encryption on gpus. In *2020 IEEE International Symposium on Workload Characterization (IISWC)*, page 264–275. IEEE, October 2020.
- [41] Sangpyo Kim, Jongmin Kim, Michael Jaemin Kim, Wonkyung Jung, John Kim, Minsoo Rhu, and Jung Ho Ahn. Bts: An accelerator for bootstrappable fully homomorphic encryption. In *Proceedings of the 49th Annual International Symposium on Computer Architecture*, ISCA '22, page 711–725, New York, NY, USA, 2022. Association for Computing Machinery.
- [42] Sangpyo Kim, Jongmin Kim, Michael Jaemin Kim, Wonkyung Jung, John Kim, Minsoo Rhu, and Jung Ho Ahn. Bts: An accelerator for bootstrappable fully homomorphic encryption. In *Proceedings of the 49th Annual International Symposium on Computer Architecture*, ISCA '22, page 711–725, New York, NY, USA, 2022. Association for Computing Machinery.
- [43] Ovunc Kocabas, Tolga Soyata, Jean-Philippe Couderc, Mehmet Aktas, Jean Xia, and Michael Huang. Assessment of cloud-based health monitoring using homomorphic encryption. In *2013 IEEE 31st International Conference on Computer Design (ICCD)*, pages 443–446. IEEE, 2013.
- [44] Wai-Kong Lee, Sedat Akleylek, Denis Chee-Keong Wong, Wun-She Yap, Bok-Min Goi, and Seong-Oun Hwang. Parallel implementation of nussbaumer algorithm and number theoretic transform on a gpu platform: application to qtesla. *J. Supercomput.*, 77(4):3289–3314, April 2021.
- [45] Vadim Lyubashevsky. Lattice signatures without trapdoors. In David Pointcheval and Thomas Johansson, editors, *Advances in Cryptology – EUROCRYPT 2012*, pages 738–755, Berlin, Heidelberg, 2012. Springer Berlin Heidelberg.
- [46] Chiara Marcolla, Victor Sucasas, Marc Manzano, Riccardo Bassoli, Frank H. P. Fitzek, and Najwa Aaraj. Survey on fully homomorphic encryption, theory, and applications. *Proceedings of the IEEE*, 110(10):1572–1609, 2022.
- [47] Christian Vincent Mouchet, Jean-Philippe Bossuat, Juan Ramón Troncoso-Pastoriza, and Jean-Pierre Hubaux. Lattigo: A multiparty homomorphic encryption library in go. In *Proceedings of the 8th Workshop on Encrypted Computing and Applied Homomorphic Cryptography*, pages 64–70, 2020.
- [48] NVIDIA. Nvidia a100 specifications, 2024.
- [49] Adiwena Putra, Prasetyo, Yi Chen, John Kim, and Joo-Young Kim. Strix: An end-to-end streaming architecture with two-level ciphertext batching for fully homomorphic encryption with programmable bootstrapping, 2023.
- [50] Brandon Reagen, Woo-Seok Choi, Yeongil Ko, Vincent T. Lee, Hsien-Hsin S. Lee, Gu-Yeon Wei, and David Brooks. Cheetah: Optimizing and accelerating homomorphic encryption for private inference. In *2021 IEEE International Symposium on High-Performance Computer Architecture (HPCA)*, pages 26–39, 2021.
- [51] Xuanle Ren, Zhaohui Chen, Zhen Gu, Yanheng Lu, Ruiguang Zhong, Wen-Jie Lu, Jiansong Zhang, Yichi Zhang, Hanghang Wu, Xiaofu Zheng, Heng Liu, Tingqiang Chu, Cheng Hong, Changzheng Wei, Dimin Niu, and Yuan Xie. Cham: A customized homomorphic encryption accelerator for fast matrix-vector product. In *2023 60th ACM/IEEE Design Automation Conference (DAC)*, pages 1–6, 2023.
- [52] M. Sadegh Riazi, Kim Laine, Blake Pelton, and Wei Dai. Heax: An architecture for computing on encrypted data. In *Proceedings of the Twenty-Fifth International Conference on Architectural Support for Programming Languages and Operating Systems*, ASPLOS '20, page 1295–1309, New York, NY, USA, 2020. Association for Computing Machinery.
- [53] Nikola Samardzic, Axel Feldmann, Aleksandar Krastev, Srinivas Devadas, Ronald Dreslinski, Christopher Peikert, and Daniel Sanchez. F1: A fast and programmable accelerator for fully homomorphic encryption. In *MICRO-54: 54th Annual IEEE/ACM International Symposium on Microarchitecture*, MICRO '21, page 238–252, New York, NY, USA, 2021. Association for Computing Machinery.
- [54] Nikola Samardzic, Axel Feldmann, Aleksandar Krastev, Nathan Manohar, Nicholas Genise, Srinivas Devadas, Karim Eldefrawy, Chris Peikert, and Daniel Sanchez. Craterlake: A hardware accelerator for efficient unbounded computation on encrypted data. In *Proceedings of the 49th Annual International Symposium on Computer Architecture*, ISCA '22, page 173–187, New York, NY, USA, 2022. Association for Computing Machinery.
- [55] Taishin Shimada and Makoto Ikeda. High-throughput polynomial multiplier architecture for lattice-based cryptography. In *2021 IEEE International Symposium on Circuits and Systems (ISCAS)*, pages 1–5, 2021.
- [56] Taishin Shimada and Makoto Ikeda. High-throughput polynomial multiplier architecture for lattice-based cryptography. In *2021 IEEE International Symposium on Circuits and Systems (ISCAS)*, pages 1–5, 2021.
- [57] Kaustubh Shivdakar, Yuhui Bao, Rashmi Agrawal, Michael Shen, Gilbert Jonatan, Evelio Mora, Alexander Ingare, Neal Livesay, José L Abellán, John Kim, et al. Gme: Gpu-based microarchitectural extensions to accelerate homomorphic encryption. *arXiv preprint arXiv:2309.11001*, 2023.
- [58] Kaustubh Shivdakar, Gilbert Jonatan, Evelio Mora, Neal Livesay, Rashmi Agrawal, Ajay Joshi, Jose Abellan, John Kim, and David Kaeli. Accelerating polynomial multiplication for homomorphic encryption on gpus, 2022.
- [59] Sujoy Sinha Roy, Furkan Turan, Kimmo Jarvinen, Frederik Vercauteren, and Ingrid Verbauwhede. Fpga-based high-performance parallel architecture for homomorphic computing on encrypted data. In *2019 IEEE International Symposium on High Performance Computer Architecture (HPCA)*, pages 387–398, 2019.

- [60] Sujoy Sinha Roy, Furkan Turan, Kimmo Jarvinen, Frederik Vercauteren, and Ingrid Verbauwhede. Fpga-based high-performance parallel architecture for homomorphic computing on encrypted data. In *2019 IEEE International Symposium on High Performance Computer Architecture (HPCA)*, pages 387–398, 2019.
- [61] McKenzie van der Hagen and Brandon Lucia. Client-optimized algorithms and acceleration for encrypted compute offloading. In *Proceedings of the 27th ACM International Conference on Architectural Support for Programming Languages and Operating Systems, ASPLOS '22*, page 683–696, New York, NY, USA, 2022. Association for Computing Machinery.
- [62] Yinghao Yang, Huaizhi Zhang, Shengyu Fan, Hang Lu, Mingzhe Zhang, and Xiaowei Li. Poseidon: Practical homomorphic encryption accelerator. In *2023 IEEE International Symposium on High-Performance Computer Architecture (HPCA)*, pages 870–881, 2023.
- [63] Xun Yi, Mohammed Golam Kaosar, Russell Paulet, and Elisa Bertino. Single-database private information retrieval from fully homomorphic encryption. *IEEE Transactions on Knowledge and Data Engineering*, 25(5):1125–1134, 2013.
- [64] Yujia Zhai, Mohannad Ibrahim, Yiqin Qiu, Fabian Boemer, Zizhong Chen, Alexey Titov, and Alexander Lyashevsky. Accelerating encrypted computing on intel gpus, 2021.
- [65] Ye Zhang, Shuo Wang, Xian Zhang, Jiangbin Dong, Xingzhong Mao, Fan Long, Cong Wang, Dong Zhou, Mingyu Gao, and Guangyu Sun. Pipezk: Accelerating zero-knowledge proof with a pipelined architecture. In *2021 ACM/IEEE 48th Annual International Symposium on Computer Architecture (ISCA)*, pages 416–428, 2021.
- [66] Yilan Zhu, Xinyao Wang, Lei Ju, and Shanqing Guo. Fxhenn: Fpga-based acceleration framework for homomorphic encrypted cnn inference. In *2023 IEEE International Symposium on High-Performance Computer Architecture (HPCA)*, pages 896–907, 2023.

A Dedicated Optimization for Modulus within 32 bits

Within the security parameter, the choice of modulus bitwidth ($\log(q)$) is decoupled from Q and degree. Precision considerations guide the selection as follows.

Thousands-bit coefficients are handled through two levels of precision breakdown:

- RNS Decomposition: This breaks $\log(Q)$ into L limbs, with each limb having a coefficient of $\log(q)$ bits.
- Chunk Decomposition: If $\log(q)$ exceeds the native hardware precision, it is further divided into smaller chunks.

Overhead Analysis: RNS-based decomposition introduces a linear overhead, whereas chunk decomposition incurs a quadratic overhead. Therefore, minimizing $\log(q)$ through RNS decomposition is preferred. For example, using the security parameter set 6 (introduced in Tab. 6) demonstrates the benefits of this approach.

The open-sourced offline compilation code for BAT could be found at https://github.com/google/jaxite/blob/60cb6a7fae7896443be8036eb8fa6106b25c5e6e/jaxite/jaxite_lib/matrix_utils.py#L570, while the runtime code of it is https://github.com/google/jaxite/blob/60cb6a7fae7896443be8036eb8fa6106b25c5e6e/jaxite/jaxite_lib/matrix_utils.py#L616.

Algorithm 4 CROSS Dedicated Mapping for 28-bit Modulus

Require: modulus q of $\log q$ bits, $a, b, c \in \mathbb{Z}_q$ with $\log q$, $\log q$, $2 \log q$ bits, hardware bit precision bp

- 1: $K \leftarrow \lceil \frac{\log q}{bp} \rceil$ ▷ Number of chunks (4 in our configuration)
- 2: **procedure** HPSCALARMULT-CONV(a, b) $\rightarrow z$ ▷ $z = a \times b$
- 3: $[a^k]_{0 \leq k < K} \leftarrow \text{CHUNKDECOMPOSE}(a)$
- 4: $[b^k]_{0 \leq k < K} \leftarrow \text{CHUNKDECOMPOSE}(b)$
- 5: $[c^i]_{0 \leq i < 2K-1} = \text{1DCONV}([a^k]_{0 \leq k < K}, [b^k]_{0 \leq k < K})$
- 6: $z += c^i \ll (bp * i)$ for $0 \leq i < 2K - 1$
- 7: **end procedure**
- 8: **procedure** BAT(b) $\rightarrow \hat{b}_i^j$ ▷ offline compilation
- 9: $[b^k]_{0 \leq k < K} \leftarrow \text{CHUNKDECOMPOSE}(b)$
- 10: ▷ 1D-IM2COL converts $[b^k]$ into a matrix
- 11: $[h_{ij}]_{0 \leq i < K, 0 \leq j < 2K-1} \leftarrow \text{IM2COL}([b^k], \text{kernel_size}=(K,))$
- 12: $\hat{b}_i^j \leftarrow h_{ij}$ **for** $0 \leq i, j < K$
- 13: **for** $0 \leq i < K$ **do**
- 14: $c_i \leftarrow 0$
- 15: **for** $K \leq j < 2K - 1$ **do**
- 16: $c_i += h_{ij} * 2^{bp(i+j-K)}$
- 17: **end for**
- 18: **do** ▷ redistribute chunks of higher bases
- 19: $c_i *= 2^{bp*K}$
- 20: $[c^k]_{0 \leq k < K} \leftarrow \text{CHUNKDECOMPOSE}(c_i \bmod q)$
- 21: $[\hat{b}_i^k]_{0 \leq k < K} += [c^k]_{0 \leq k < K}$
- 22: $[\hat{b}_i^k]_{0 \leq k < K}, c_i \leftarrow \text{CARRYPROP}([\hat{b}_i^k]_{0 \leq k < K})$
- 23: **while** $c_i \neq 0$
- 24: **end for**
- 25: **end procedure**
- 26: **procedure** HPSCALARMULT-BAT(a, b) $\rightarrow z$ ▷ $z = a \times b$
- 27: $[a^k]_{0 \leq k < K} \leftarrow \text{CHUNKDECOMPOSE}(a)$
- 28: $[\hat{b}_i^j]_{0 \leq i, j < K} \leftarrow \text{BAT}(b)$
- 29: $[c^j]_{0 \leq j < K} = [\hat{b}_i^j]_{0 \leq i, j < K} \times [a^j]_{0 \leq j < K}$
- 30: $z += c^j \ll (bp * j), 0 \leq j < K$
- 31: **end procedure**
